FY 2019 Master Thesis

# High Temperature deformation of additively manufactured porous titanium with ordered cell structures

January 24, 2020

Department of Aeronautics and Astronautics
Graduate School of Systems Design
Tokyo Metropolitan University

Student number: 18863638 Shiyue GUO

Thesis supervisor Koichi KITAZONO

This study consists of five chapters as follows.

Chapter 1: Titanium and its alloys have been widely used as aviation, aerospace and biomedical materials duo to their superior mechanical properties, light weight, high temperature resistance, high strength, biochemical compatibility, low elastic modulus and corrosion resistance. Due to the excellent properties of porous metal in terms of weight reduction and energy absorbers, sound absorbers, heat transfer and high specific stiffness with low specific weight, at present, porous metal materials are increasingly attracting researchers' attention in light metal materials. Especially in the aerospace industries, automotive industry, construction industry, military industry, biological implant materials etc. Different from the traditional manufacturing methods of metal foam, for example, melt foaming, casting and chemical or physical deposition of metal, the research on the manufacturing method of porous materials mainly focuses on powder metallurgy (PM) and additive manufacturing (AM). Porosity, unit cell such as honeycomb, cubic, diamond, rhombic dodecahedron and truncated octahedron, compression temperature and compression rate have important effects on the compression characteristics during deformation of AM porous titanium. However, the influence of cell structure and relative density on the temperature dependence of AM porous titanium was ignored. Based on previous research results that the PM Titanium foam is less temperature dependent than the commercial pure titanium.

The purpose of this study is to analyze the effect of cell structure and porosity on temperature dependence by comparing the activation energy of porous titanium and titanium foam with different porosity.

Chapter 2: The compression behavior of commercial pure titanium porous structure with a cell shape truncated octahedron, which was fabricated by Additively manufactured technique using electron beam melting, was investigated at different temperature and strain rate. A series of quasi-static compression tests were performed at ambient temperature, 300K, 473K and 673K with different strain rate of $5.6*10^{-3}s^{-1}$, $5.6*10^{-4}s^{-1}$ and $5.6*10^{-5}s^{-1}$ at porosity of 85%, 92% with Shimadzu Autograph AG-50kNISD and CONCRETO 2000X, respectively.

Truncated octahedron open-cell geometries are constructed by 3D-Voronoi. And the schematic illustration of the 3D-Voronoi procedure for porous structure generation is described in detail in the following sections. The compression specimens were prepared with a diameter of 30mm and height of 30mm cylinder and cell structure is truncated octahedron with the thickness is 1mm. The condition of electron beam melting by the electron beam output is 210W and the scanning speed is 232.4mm/s with Arcam A2X machine.

Chapter 3: The compressive deformation behavior of AM porous titanium with different loading direction. The compressive deformation behavior of AM porous titanium with different strain rate. The compressive deformation behavior of AM porous titanium with different compressive temperature. Obtaining stress-strain curves under different conditions and get the corresponding plateau stress from the stress-strain curve.

Chapter 4: The results revealed the occurrence of shear bands is related to the properties of material,

the different deform mechanism of cell struct and the compressive temperature. The reason why anisotropy occurs is the number of structs parallel, vertical, and diagonal to the compression direction is different. According to numerical simulation of cell structure, it can be obtained that the deform domination of oblique structs of bcc-Voronoi[001] is yielding dominated, oblique structs of bcc-Voronoi[011] is yielding dominated and parallel structs is buckling dominated, oblique structs bcc-Voronoi[111] is bending dominated. And the anisotropy of AM porous titanium was unchanged with the temperature and porosity duo to deform mechanism unchanged. The value of the strain rate sensitivity and the activation energy of porous titanium were compared with titanium foam and dense titanium. The m-value of PM foam titanium is 0.018. The m value of AM porous titanium with porosity of 85% is 0.020 and the m-value of 92% is 0.014 which is almost equal than those of PM titanium foam at room temperature. The low strain rate sensitivity is due to the property of titanium. It can be concluded that the porosity of titanium has a limited effect on strain rate sensitivity. But the rate sensitivity deviation between titanium foam, commercial pure titanium and porous titanium is mainly caused power low breakdown at temperature of 473K. The strain rate sensitivity was quite low since it was affected by property of material. The value of the activation energy between 300 to 673 K was 515kJ/mol with porosity of 85% and 502kJ/mol with porosity of 92% lower than those of dense titanium (746kJ/mol) and powder metallurgically manufactured titanium foam (603kJ/mol) with low porosity. This is because the dominant deformation mode of the AM porous titanium (bcc-Voronoi [011]) specimens are yielding and buckling of thin cell edges. While the deform mechanism of titanium foam is yielding-dominant and bending-dominant of cell structs.

Chapter 5: Compression tests of AM porous titanium specimens with bcc-Voronoi cell structure were carried out with different strain rates, temperatures and compression directions. The conclusion is as follows:

Ordered open-cell porous metal has obvious anisotropy, and the anisotropy of ordered open-cell porous titanium is not affected by temperature and porosity. The occurrence of shear bands is related to the properties of the material and deform mechanism of cell structs. And the higher the brittle and the lower the ductility, the easier it is to occur shear bands. The strain rate sensitivity is low at the low strain rate. The change of m is affected by the porosity at the same temperature duo to the power-law breakdown, and m also changes with the temperature at same porosity duo to the strain enhancement mechanism may change. The temperature dependence of the disordered structure is higher than that of the ordered structure, because the low activation energy is due to the dominant deformation mode of bending and buckling.

In the future, it will be further verified that the activation energy of porous titanium is affected by the deformation mechanism of cell structs, rhombic dodecahedron and diamond. And their corresponding irregular structures will be accepted on the compression tests.

# Content

# 1. Introduction

## 1.1 Porous metal

Due to the global warming and excessive consumption of fossil energy caused by carbon dioxide emissions in recent years, various environmental problems have caused people to pay more and more attention to environmental pollution. Porous materials, as a new structural and functional material, compared with solid materials, porous materials can exert excellent comprehensive mechanical properties under lightweight. In the past, porous materials have been limited in their applications due to manufacturing technology and economic reasons. Due to the diversification of manufacturing methods, maturity and high efficiency, porous materials have been rapidly developed in recent years and in the future. Porous metal has been the focus of research by researchers over the past two decades, but in addition to its cost advantages, porous metal has many inevitable defects, such as a wavy deformation of cell walls, changes in cell wall thickness, and uneven cell shape. And because of the existence of these defects, the mechanical properties of the porous metal are unstable, so the development of porous metal in the future has limitations. Porous metals have good physical, mechanical, thermal, electrical and acoustic properties and are embodied in the lightweight structure of porous metals, high specific strength, energy absorption, high gas permeability and high thermal conductivity [1]. Although porous metals are not dominant in terms of cost, the mechanical properties of porous metals are stable and controllable, so porous metals are increasingly favored by researchers.

According to the cell structure, the metal foam can be classified into an open-cell metal foam and a closed-cell metal foam. All the pores are joined together in a network structure called open-cell foam metal (Fig. 1.1), and the foam metal whose pores are completely surrounded by a thin metal wall or film is classified as a closed metal foam (Fig. 1.2) [1].

Fig. 1.1 Section of closed-cell foam

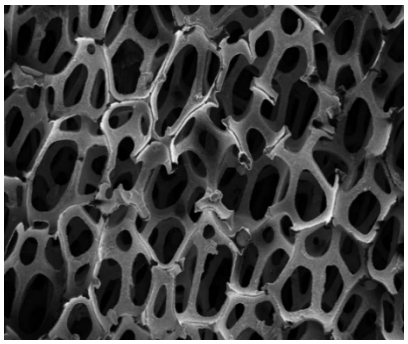

Fig. 1.2 Section of open-cell foam

### 1.2 The application of porous metal

Porous metal is widely application in the aerospace industry, automotive industry construction industry, biological implant materials since its excellent energy absorption and lightweight with high strength.

#### 1.2.1 Aerospace industry

Previous research in the aerospace field has mainly utilized the lightweight of foam metal, which has played an important role in reducing weight and saving fuel for spacecraft such as rockets, thereby reducing launch costs and protecting the environment. For example, the application of aluminum foam sandwiches on the nose cone of Ariane 5 [3]. And due to its high strength, lightweight and excellent energy absorption properties, porous metals can be used well in the development of spacecraft in the future, such as the wing of a civil aircraft, the lunar or the landing of Mars.

#### 1.2.2 Automobile industry

In the automotive field, the use of lightweight porous metal to reduce the quality of the car to reduce energy consumption and the use of excellent energy absorption performance to protect the driver in the event of high-speed collisions. Especially in today's high-speed railway development, it is especially important to minimize the damage to passengers during an accident [4].

#### 1.2.3 Chemical industry

Porous metal has excellent thermal conductivity in the chemical industry, such as can be used as catalysts and catalyst support due to their large specific surface area [5]. Fig. 1.3 shows the open cell AlSi7Mg foam probes used for the heat transfer.

Fig. 1.3 Open cell AlSi7Mg foam probes used for the heat transfer.

### 1.2.4 Biological implant materials

Due to the complex structure of the human environment, medical implants are generally required to have suitable biocompatibility, mechanical properties, strength, corrosion resistance, and elastic modulus [6]. Titanium and its titanium alloys are widely used in biomedical applications in foam metals, mainly because of their high strength, biocompatibility and excellent corrosion resistance [7]. Porous metal will significantly reduce stress shielding due to the higher elastic modulus of dense metals than bones, while the porous structure provides a space for bone tissue in growth. Fig. 1.4 shows (a) Tantalum trabecular metal tibial baseplate for uncemented total knee replacement. (b) X-ray shows implant osseointegration at 1 year of follow-up.

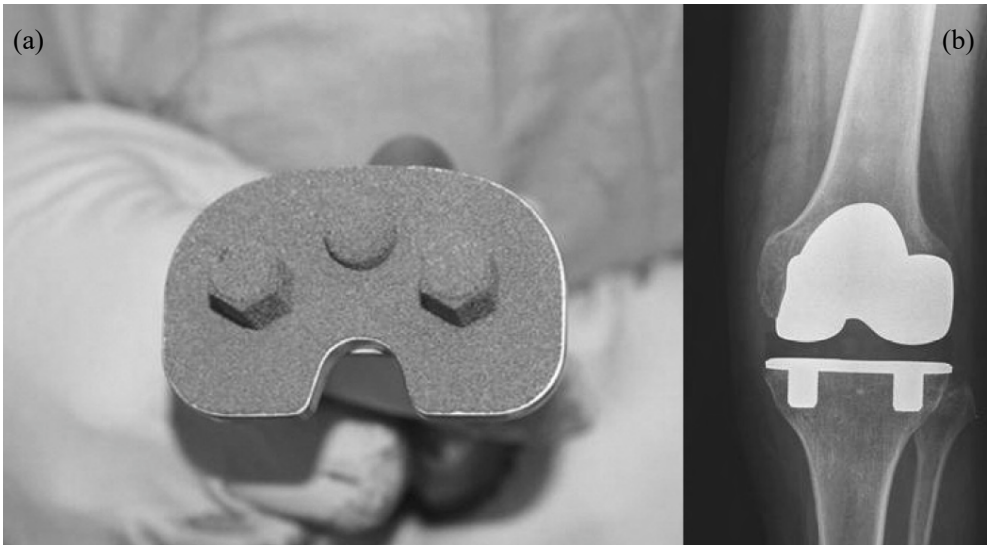


Fig. 1.4 (a) Tantalum trabecular metal tibial baseplate for uncemented total knee replacement. (b) X-ray shows implant osseointegration at 1 year of follow-up[7)].

### 1.3 The manufactured porous metal

#### 1.3.1 Summary of traditional manufacturing methods

Porous materials have grown considerably over the past decade as a novel material. The continuous development of high-tech industry technology has put increasing requirements on the variety, quality and performance of porous metal materials. There are many traditional methods for preparing metal foam. Depending on the internal pore structure, they can be divided into two categories: closed-cell foam metal and open-cell foam metal. The preparation method is mainly a casting method and a sintering method [8, 9]. Powder metallurgy, as a method of manufacturing porous materials, is rapidly developed due to its low cost and ability to produce complex structures, high porosity, and relatively uniform porous materials[10]. The unstable performance of the porous structure produced by powder metallurgy is mainly due to the performance of the porous metal produced by powder metallurgy mainly affected by the content and distribution of the foaming agent, compaction pressure and temperature. The traditional manufactured method of open-cell structures can be controlled the cell structures; high added value, complex preparation processes, and relatively difficult production in large-scale production; difficult to control pore structures; and the production of closed-cell structures has low added value; simple production processes, and relatively easy production. Different from the traditional manufacturing methods of metal foam, for example, melt foaming, casting, powder metallurgy and chemical or physical deposition of metal, the research on the manufacturing method of porous materials mainly focuses additive manufacturing. And compared with subtractive manufacturing, AM is particularly suitable for producing low volumes of products, especially for parts with complex geometries [11].

### 1.3.2 Additive manufacturing

Additive manufacturing (AM) technology has been researched and developed for more than 20 years and provide an exceptional opportunity for manufacturing porous material to appliances. Additive manufacturing has been favored by researchers for its superior design freedom and efficient delivery time over the past decade. The immature technology at the beginning limited the rapid development of additive manufacturing, but as technology advances, it can achieve very high porosity, very complex and evenly distributed pore structure, stable porous materials, such as aluminum, steel and Titanium-based parts or structures. The following review AM applications in the aerospace, automobile, biomedical and energy fields [11].

Additive manufacturing (AM) is based on taking a 3D geometry, slicing it to multiple layers, and a layer-by-layer construction of parts to create 3D parts directly from CAD models. There STL (standard Tessellation Language) may not be suitable for complex operation and precision, therefore many AM technologies are using solid models as input. According to the ASTM International Committee, additive manufacturing can be classified into two categories: direct energy deposition (DED)and powder bed fusion (PBF)[11]. DED includes direct metal deposition (DMD), laser engineered net shaping (LENS), direct manufacturing (DM), shaped metal deposition or wire and arc additive manufacturing (WAAM). PBF includes selective laser sintering (SLS), direct metal laser sintering (DMLS), laser melting (LM), selective laser melting (SLM) and electron beam melting (EBM)[11]. PBF advantages are building of complex, hollow cooling passages, and high precision parts, while the disadvantages are building envelope, single material per build and horizontal layer building ability. And DED offer larger building envelope and higher deposition rate, while there are limited by ability of building hollow cooling passages and finer geometry[11]. The following specifically introduces the process of SLM and EBM.

#### 1.3.2.1 Selective laser melting

Selective laser melting is a powder bed-based process that occurs in a process chamber filled with an inert gas atmosphere. The SLM is carried out by the laser beam generated by the continuous wave mode laser beam passing through the deposited powder layer at a certain scanning speed, and then according to the cross section of the part, the metal powder is selectively exposed to the laser beam. After the powder bed is selectively exposed to the laser beam, the contour of the part is completely melted, followed by another powder layer, and finally the new deposition is repeatedly melted. The process of powder layer until the completion of the part [12]. SLM can process a range of a metal including titanium which are desirable for appliances requiring high specific strength. Fig. 1.5 Schematics of an SLM machine. Fig. 1.6 shows a photograph of porous Ti-6Al-4V manufactured by SLM.

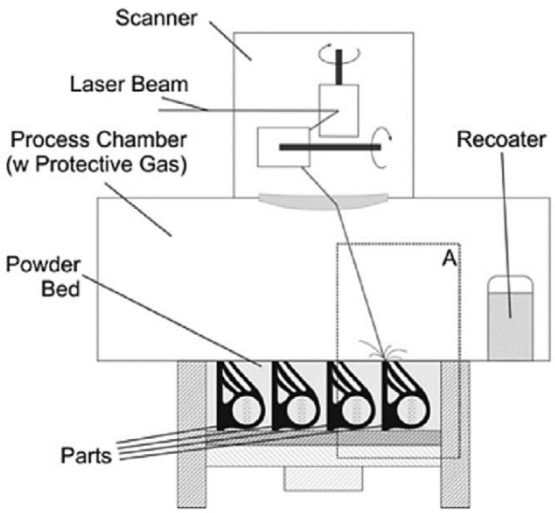


Fig. 1.5 Schematics of an SLM machine.

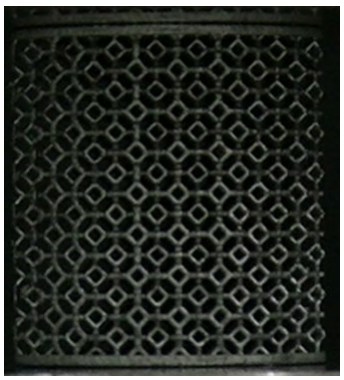

Fig. 1.6 Photograph of porous Ti-6Al-4V manufactured by SLM

#### 1.3.2.2 Electron beam melting

As with the SLM process, the EBM process must also establish a powder bed, but unlike the SLM process, the EMB process uses a heat source that is an electron beam and scans much faster than SLM and EBM offer the advantage of low residual stress as compared to laser based system. Steps of the EBM process: First, the electron beam repeatedly scans the metal powder at a rapid scanning speed for preheating the powder; then lowering the scanning speed for the metal powder to completely melt; finally repeating the powder dispersion until the part is completed. In order to avoid the charging of the powder particles and enhance the heat conduction and cooling of the melt, the input of helium during the melting process increases the pressure atmosphere inside the operating system from a vacuum to a certain extent [12)] (Fig. 1.7). Fig. 1.8 shows the photograph of porous titanium manufactured by EBM.

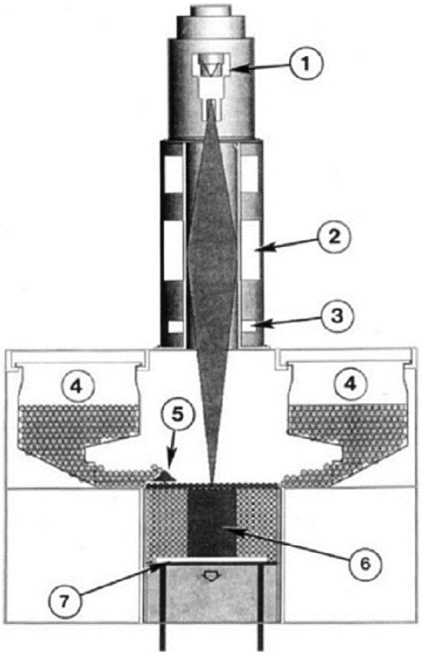


Fig. 1.7 Schematics of an EBM machine[12]. 1: electron gun, 2: lens system, 3: deflection lens, 4: powder cassettes with feedstock, 5: rake, 6: building component, 7: build table.

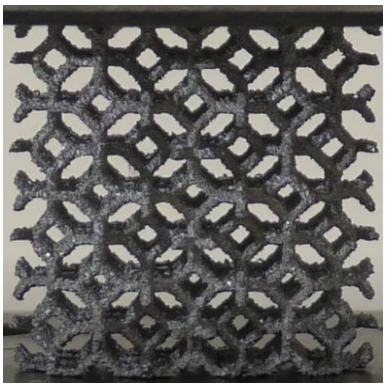

Fig. 1.8 Photograph of porous titanium manufactured by EBM.

### 1.4 Previous research

Porous materials of different materials have been previously studied, for example gold material [13], magnesium material [14], copper material [15], aluminum material [16], stainless steel material [17] and titanium material [18].

#### 1.4.1 The mechanical properties of Titanium

The reserves of titanium resources on the earth are abundant, so the development of high value-added titanium and titanium alloys has become the focus of attention in recent years. The development of titanium and titanium alloys has been more than fifty years, especially in the past two decades, the technical maturity and cost reduction of the preparation of titanium and titanium alloys. Compared with other metals, titanium has excellent physical and chemical properties such as low specific gravity, high strength, corrosion resistance, fatigue resistance, heat resistance, low coefficient of thermal expansion, low thermal conductivity, low temperature brittleness, wear resistance and biocompatible [19, 20]. Therefore, titanium and titanium alloys are widely used, mainly in the base parts of the aerospace and automotive fields, heat exchangers in the petrochemical industry, and bone materials in the medical field [11, 22]. However, the use cost of titanium is very high compared with aluminum and steel, so it is feasible to improve the use efficiency of titanium.

#### 1.4.2 The previous research of mechanical properties of porous titanium

The mechanical performance of porous materials is dependent on cell geometric; cell strut diameter; material and manufacturing process characteristics; as well as loading conditions such as strain rate and temperature. Fig. 1.9 shows Photograph of a titanium foam specimen fabricated by Powder metallurgy of side 22 mm. Fig. 1.11 3D-CAD images of the unit-cells of (a) Truncated octahedron, (b) Rhombic. Fig. 1.12 The compressive stress-strain curve of porous titanium at different porosity. Fig. 1.13 The compressive stress-strain curve of porous titanium at different cell structure. According to

previous research results, the mechanical properties of porous titanium are mainly determined by the manufacturing method, porosity, cell geometries, compression speed, and compression direction [23-27]. According to the relationship between the plateau stress and the relative density, it can be known that the platform stress increases with the increase of the relative density; the influence of the pore structure on the platform stress is mainly the shape and quantity of the enthalpy and the compression direction; and the platform stress also follows due to the high temperature softening. The compression temperature is lowered and lowered; and according to the research results, the porous titanium manufactured by powder metallurgy is less temperature dependence than CP-titanium [28] (Fig. 1.10).

Fig. 1.9 Photograph of a titanium foam specimen fabricated by Powder metallurgy of side 22 mm.

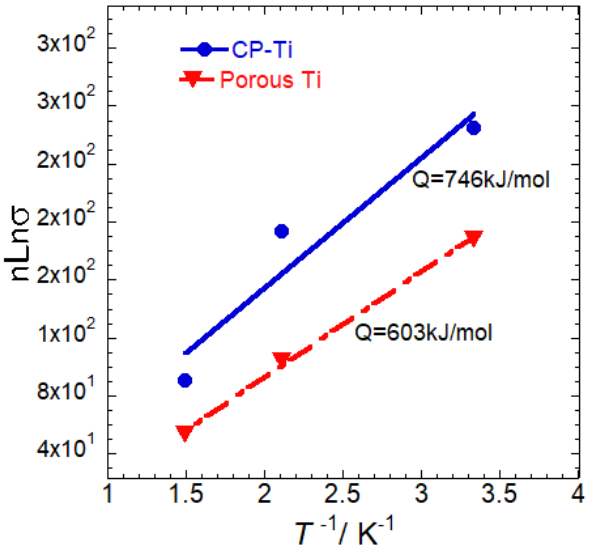


Fig. 1.10 Relationship of the logarithmic plot of flow stress and 1/T linear curves.

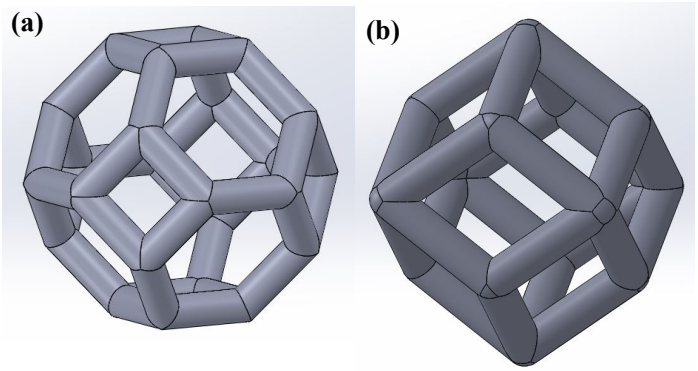


Fig. 1.11 3D-CAD images of the unit-cells of (a)Truncated octahedron, (b) Rhombic.

dodecahedron.

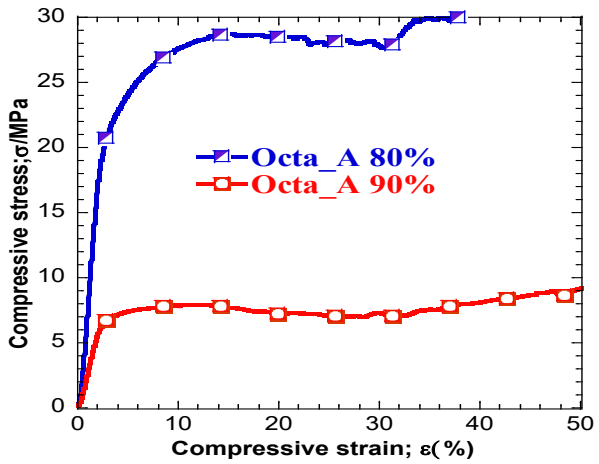


Fig. 1.12 The compressive stress-strain curve of porous titanium at different porosity.

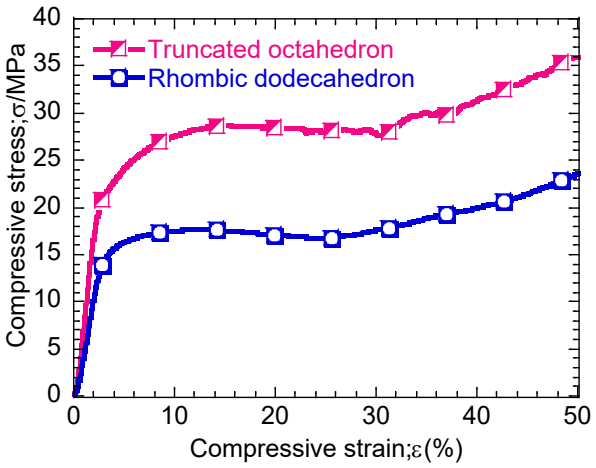


Fig. 1.13 The compressive stress-strain curve of porous titanium at different cell structure.

### 1.5 The purpose of this study

The purpose of this study is to analyze the effect of loading direction, strain rate and compressive temperature on the compression behavior of AM porous titanium.

## 2. Experimental procedure

This sample is a porous titanium made of industrial pure titanium by 3D additive manufacturing and subjected to a compression test at room temperature and high temperature to evaluate temperature dependency. Truncated octahedron open-cell geometries are constructed by 3D-Voronoi used RHINO.6.

### 2.1 3D-Voronoi

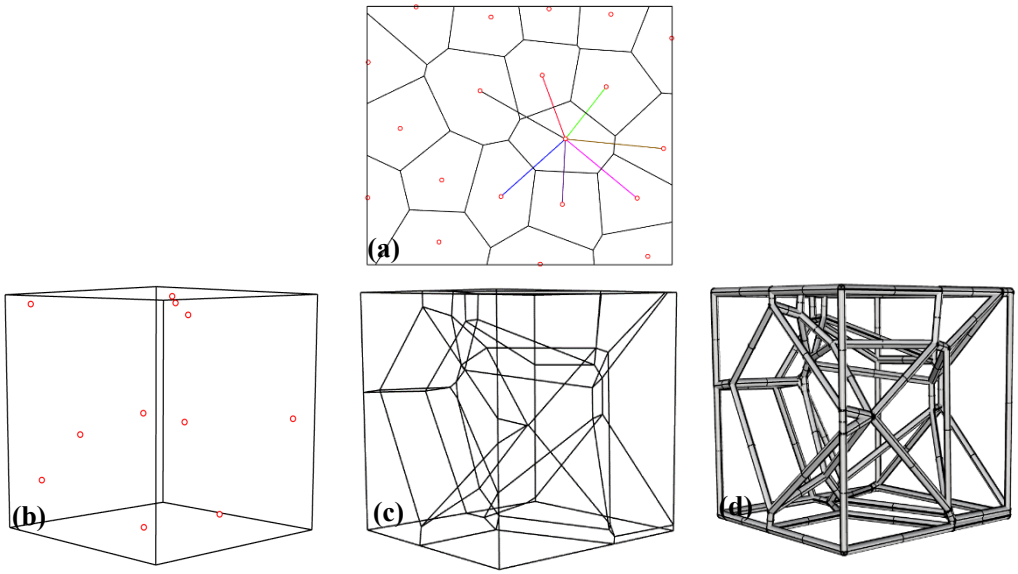


Fig. 2.1 The schematic illustration of the procedure for porous structure generation. (a) 2D-Voronoi diagram (space division by vertical bisectors of neighboring generating points); (b)(c)(d) 3D-Voronoi diagram.

In the case of open-cell porous structure, by having a set of n seed points representing the centers of m-dimensional space, the Voronoi tessellation technique can be used to link all the points in that space with nearest seed points, generating n regions that form the Voronoi diagram, and division of space by vertical bisectors of neighboring generating points [29]. The schematic illustration of the procedure of Voronoi is shown Fig. 2.1.

### 2.2 The product procedure of truncated octahedron by 3D-Voronoi

It can be known from the Eq. 1 that the porosity depends on the thickness of strut and length of strut.

$$p = 1 - \frac{3\sqrt{2}}{16}\pi\left(\frac{a}{t}\right)^{-2} \quad (1)$$

Where p is the porosity of AM porous titanium; a is the strut length; t is the thickness of strut.

The schematic illustration of the procedure for Truncated octahedron generation are shown in Fig. 2.2. Depending on the compression direction (Fig. 2.3a), the truncated octahedron open-cell geometries can be divided into bcc- Voronoi [001] (Fig. 2.3b), bcc-Voronoi [011] (Fig. 2.3c), bcc-Voronoi [111] (Fig. 2.3d).

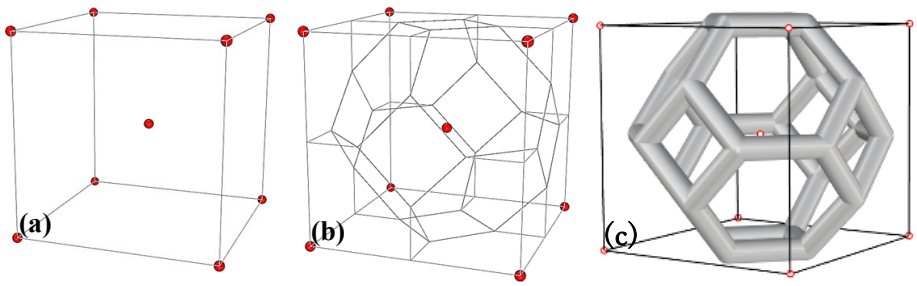


Fig. 2.2 The schematic illustration of the procedure for Truncated octahedron generation.

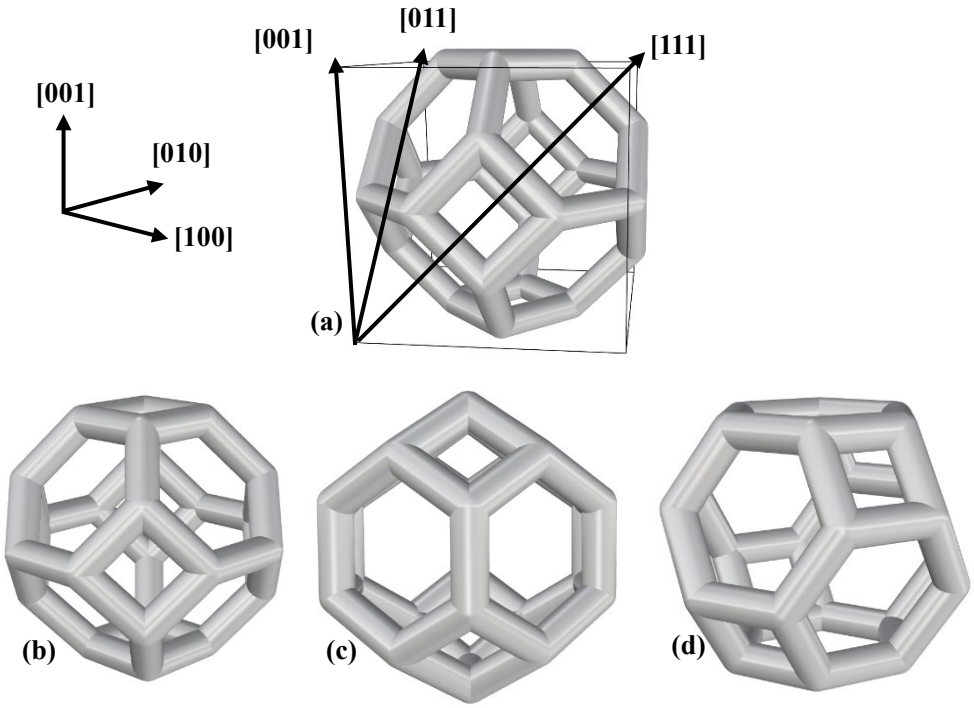


Fig. 2.3 3D-CAD images of the unit-cells of (a) bcc-Voronoi [001], (b) bcc-Voronoi [011] and (c) bcc-Voronoi [111].

**2.3 Preparation of specimen**

Open-cell porous titanium with different porosities and cell geometries were manufactured by electron beam melting and electron beam output was 210W, the scanning speed was 232.4mm/s. The sample was manufactured by using Arcam A2X machine (Fig. 2.4). Commercial pure titanium, Grade 2, powder was used as base metal. The chemical composition is shown in Table 1. The shape of the specimen is a diameter of 30mm and height of 30mm cylinder. The cell geometry is truncated octahedron with the thickness is 1mm. Fig. 2.6 shows the photographs of AM porous titanium specimens. Deviation between theoretical value of 3D model and actual value of specimen. The porosity theory of the 3D model designed by Eq. 1 is 85% and 90%, but the porosity of the specimens actually measured are 85% and 92%, mainly because the surface of the 3D model is smooth and different from the 3D model, the surface of the specimen fabricated by EBM is rough. Fig. 2.5 shows the SEM image of AM porous titanium for the individual strut at a porosity of 85%. The building

direction of specimen and the compression direction of specimens are parallel in this experiment.

Table 2.1 Chemical composition of commercially pure titanium,

| **Element** | **C** | **Fe** | **0** | **N** | **H** | **Ti** |
|---|---|---|---|---|---|---|
| **Mass (%)** | 0.01 | 0.08 | 0.13 | 0.004 | 0.001 | Bal. |


Fig. 2.4 Arcam A2X machine as electron beam melting process.

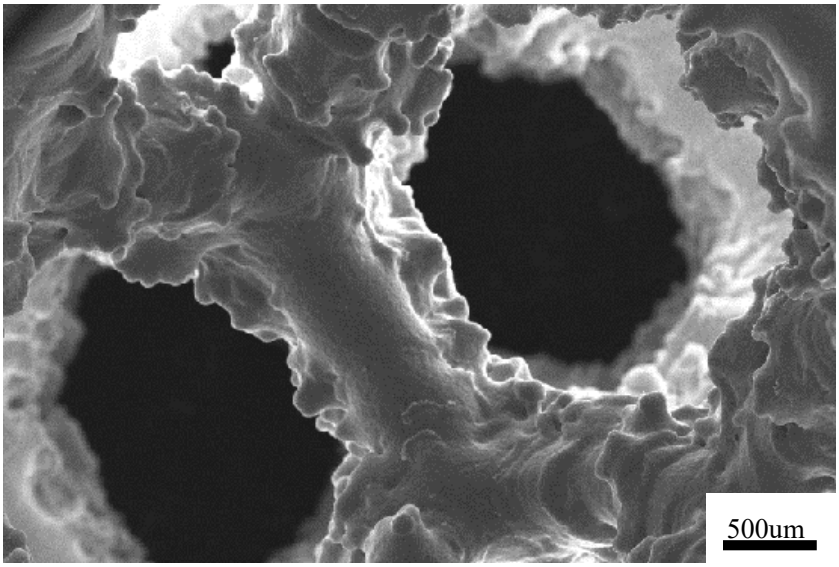


Fig. 2.5 The SEM image of AM porous titanium for the individual strut at porosity of 85%.

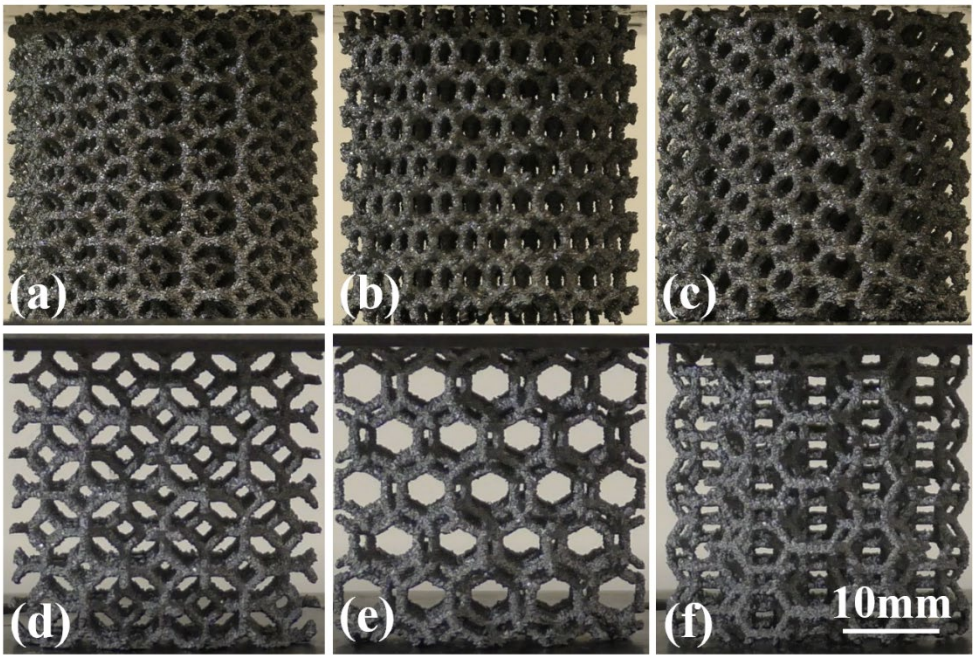


Fig. 2.6 Photographs of AM porous titanium specimens. Porosities are (a)-(c) 85% and (d)-(f) 92%. Cell structures are bcc-Voronoi (a) (d) [001], (b) (e) [011], (c) (f) [111].

**2.4 The condition of compression test**

Porous titanium specimens were carried out at room temperature using a Shimadzu Autograph AG-50kNISD (Fig. 2.7) and high temperature using a CONCRETO 2000X (Fig. 2.8). The test conditions of compressive experimental were at strain rate of $5.6*10^{-3}$ $s^{-1}$, $5.6*10^{-4}$ $s^{-1}$, $5.6*10^{-5}$ $s^{-1}$ and compression temperature of 300 K, 473, 673K.

Fig. 2.7 Shimadzu Photograph of Autograph AG-50kNISD

Fig.2.8 Photograph of CONCRETO 2000X

## 3. Results

The relationship between the flow stress and strain rate can be expressed as,

$$\sigma = \frac{F}{A} \tag{2}$$

$$\varepsilon = \frac{l}{h} \tag{3}$$

where σ is the stress, ε is the strain, F is the download, A is the initial cross section of specimen, l is the specimen displacement, h is the initial height of specimen, m is the strain rate sensitivity, $\dot{\varepsilon}$ is the strain rate and K is the constant depending on the temperature.

### 3.1 The compressive deformation behavior of AM porous titanium with different loading direction

The representative quasi-static compressive stress versus strain curves of open-cell AM porous titanium with different loading directions are shown in Fig. 3.1 at a strain rate of $5.6*10^{-3}s^{-1}$ and compressive temperature of 300K, 473K, 673K. The stress-strain curves depict three distinct regions: (i) linear elastic region, (ii) plateau region, where the stress oscillates about the average stress values with the increase in strain, and (iii) the densification region, where the stress increases sharply with strain due to densification of cells.

Similar to existing studies on porous structure, the plateau stress from the stress-strain curve are important parameter that can evaluate the compressive behavior of open-cell AM porous titanium with different loading direction across a wide range of temperature. The plateau stress is calculated as the average value of the flow stress for the strain of 20% to 30%. The plateau stresses of bcc-Voronoi [001], bcc-Voronoi [011] and bcc-Voronoi [111] with porosity of 85% at 300K are 24.6 MPa, 19.6 MPa and 15.1MPa, respectively. The plateau stresses of bcc-Voronoi [001], bcc-Voronoi [011] and bcc-Voronoi [111] with porosity of 85% at 473K are 15.1 MPa, 11.6 MPa and 9.2 MPa, respectively. The plateau stresses of bcc-Voronoi [001], bcc-Voronoi [011] and bcc-Voronoi [111] with porosity of

85% at 673K are 6.1 MPa, 5.3 MPa and 5.1 MPa, respectively. The plateau stresses of bcc-Voronoi [001], bcc-Voronoi [011] and bcc-Voronoi [111] with porosity of 92% at 300K are 5.5 MPa, 4.8 MPa and 3.8 MPa, respectively. The plateau stresses of bcc-Voronoi [001], bcc-Voronoi [011] and bcc-Voronoi [111] with porosity of 92% at 473K are 3.4 MPa, 2.5 MPa and 1.9 MPa, respectively. The plateau stresses of bcc-Voronoi [001], bcc-Voronoi [011] and bcc-Voronoi [111] with porosity of 92% at 673K are 2.4 MPa, 1.7 MPa and 1.3 MPa, respectively. The AM porous titanium have an obvious anisotropy and the plateau stress of AM porous titanium are enhanced with decreasing the porosity, the detail will be discussed in the following section.

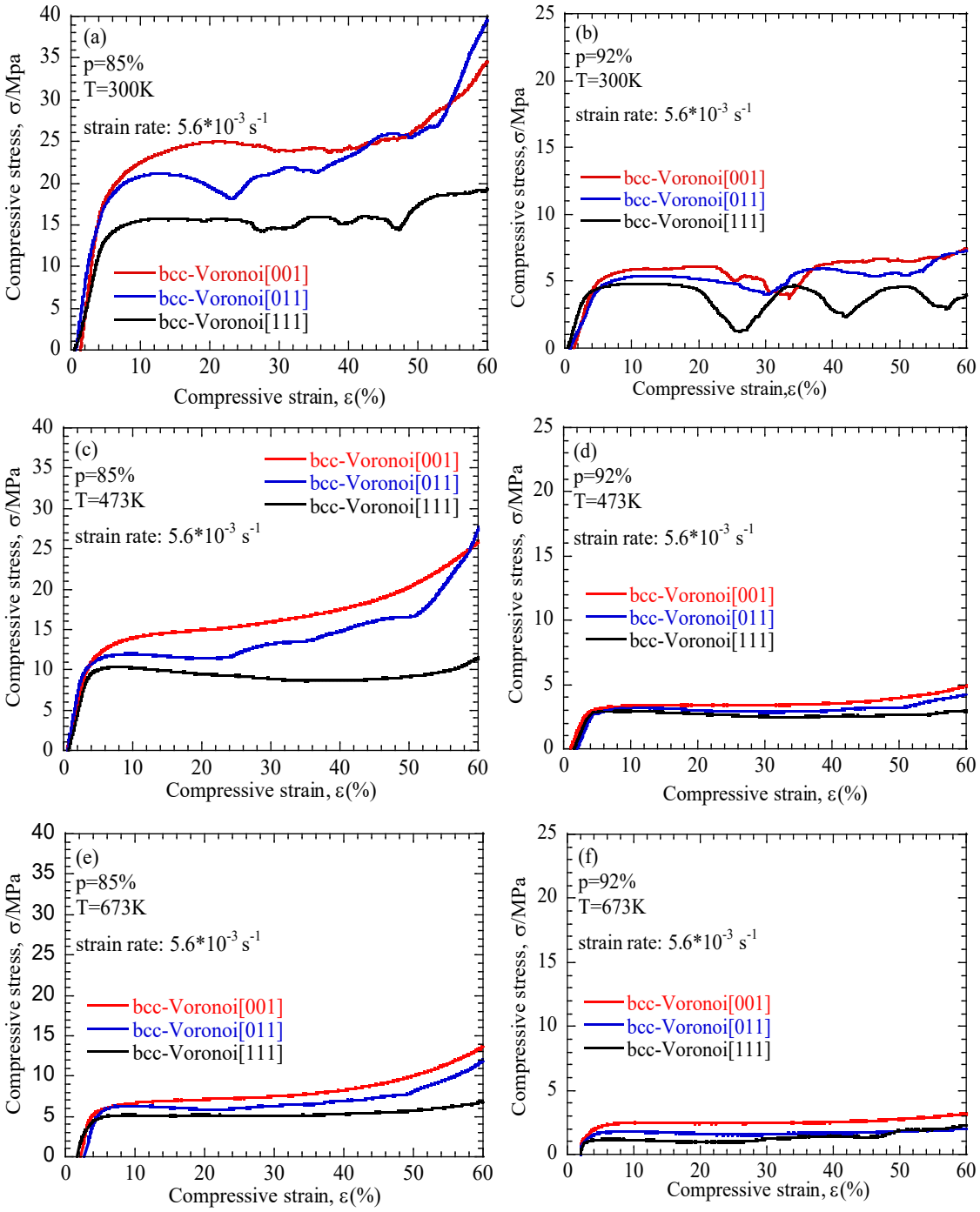


Fig. 3.1 Compressive stress-strain curves of AM porous titanium with different loading direction. (a)(c)(e) porosity of 85%; (b)(d)(f) porosity of 92%. (a)(b) temperature of 300K, (c)(d) temperature of 473K, (e)(f) temperature of 673K.

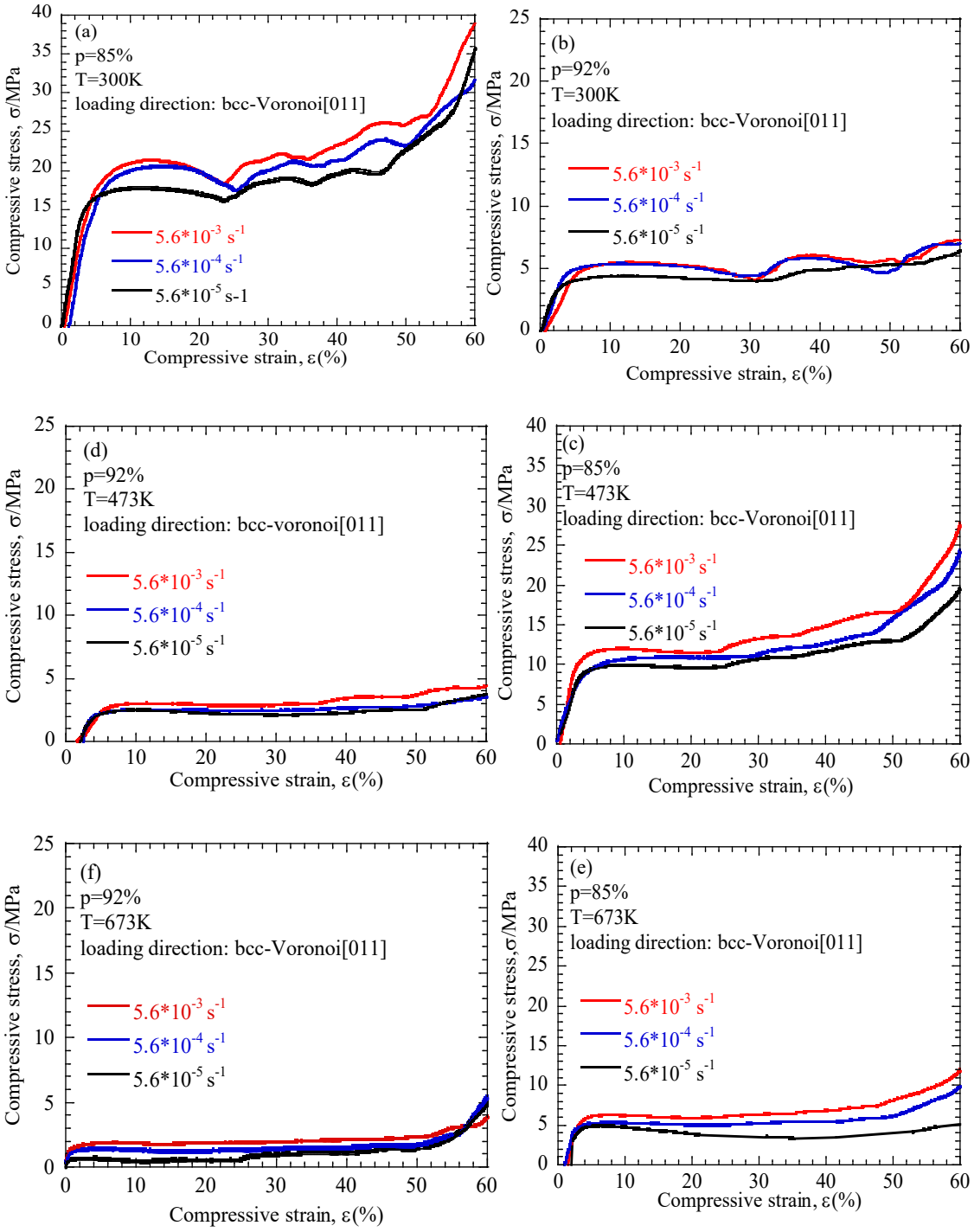


Fig. 3.2 Compressive stress-strain curves of AM porous titanium of bcc-Voronoi [011] cells with different compressive strain rate. (a)(c)(e) porosity of 85%; (b)(d)(f) porosity of 92%. (a)(b) temperature of 300K, (c)(d) temperature of 473K, (e)(f) temperature of 673K.

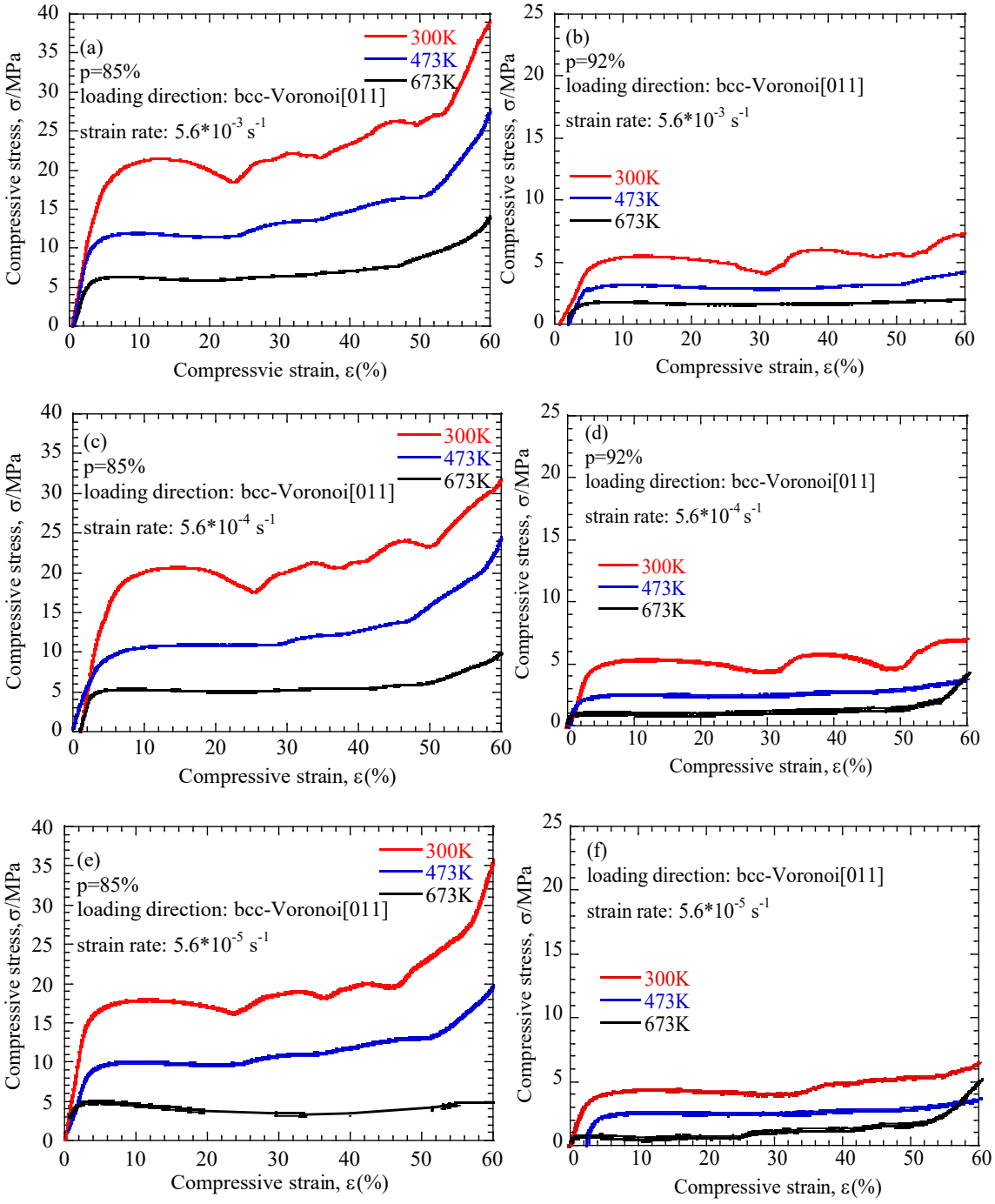


Fig. 3.3 The compressive stress-strain curves of AM porous titanium with different temperature.

(a)(c)(e) porosity of 85%; (b)(d)(f) porosity of 92%.

### 3.2 The compressive deformation behavior of AM porous titanium with different strain rate

Fig. 3.2 shows compressive stress-strain curves of AM porous titanium with three different strain rates at different temperature. When the initial strain rate is $5.6*10^{-3}$ $s^{-1}$, $5.6*10^{-4}$ $s^{-1}$and $5.6*10^{-5}$ $s^{-1}$, the plateau stresses of bcc-Voronoi [011] with porosity of 85% at 300K are 19.6 MPa, 18.8 MPa and 17.9 MPa, respectively. When the initial strain rate is $5.6*10^{-3}$ $s^{-1}$, $5.6*10^{-4}$ $s^{-1}$and $5.6*10^{-5}$ $s^{-1}$, the plateau stresses of bcc-Voronoi [011] with porosity of 92% at 300K are 4.8 MPa, 4.7 MPa and 4.5 MPa, respectively. When the initial strain rate is $5.6*10^{-3}$ $s^{-1}$, $5.6*10^{-4}$ $s^{-1}$and $5.6*10^{-5}$ $s^{-1}$, the plateau stresses of bcc-Voronoi [011] with porosity of 85% at 473K are 11.6 MPa, 10.9 MPa and 10.0 MPa, respectively. When the initial strain rate is$5.6*10^{-3}$ $s^{-1}$, $5.6*10^{-4}$ $s^{-1}$and $5.6*10^{-5}$ $s^{-1}$, the plateau stresses of bcc-Voronoi [011] with porosity of 92% at 473K are 2.5 MPa, 2.4 MPa and 2.2 MPa, respectively. When the initial strain rate is $5.6*10^{-3}$ $s^{-1}$, $5.6*10^{-4}$ $s^{-1}$and $5.6*10^{-5}$ $s^{-1}$, the plateau stresses of bcc-Voronoi [011] with porosity of 85% at 673K are 5.3 MPa, 5.1 MPa and 4.2 MPa, respectively. When the initial strain rate is $5.6*10^{-3}$ $s^{-1}$, $5.6*10^{-4}$ $s^{-1}$and $5.6*10^{-5}$ $s^{-1}$, the plateau stresses of bcc-Voronoi [011] with porosity of 92% at 300K are 1.7 MPa, 1.6 MPa and 1.4 MPa, respectively. The plateau stress of AM porous titanium increased with the elevated initial strain rate at same temperature duo to strain hardening. And the plateau stress of AM porous titanium decreased with elevated compressive temperature duo to high temperature softening.

### 3.3 The compressive deformation behavior of AM porous titanium with different compressive temperature.

Fig. 3.3 shows compressive stress-strain curves of AM porous titanium with three different compressive temperature at different loading direction. And the plateau stress of AM porous titanium decreased with elevated compressive temperature duo to high temperature softening.

## 4. Discussion

### 4.1 The anisotropy of AM porous titanium

According to previous research, it is known that the compressive strength of porous metals was affected by the porosity, cell geometries, and cell size. Yue has studied the compressive strength of truncated octahedron and rhombic dodecahedron at room temperature, and according to the research results, it is obtained that the compressive strength of porous metals increases as the porosity decreases; the compression strength of truncated octahedron is higher than that of rhombic dodecahedron [28]. However, the compressive temperature relationship and anisotropy of AM porous titanium were not clear. The obtained values of plateau stress of AM porous titanium from the compressive stress-strain curves. Fig. 4.1 shows the plateau stress of AM porous titanium plotted against the loading direction at different compressive temperature. (a) porosity of 85%; (b) porosity of 92%.

On one hand, the plateau stress changes with the compression direction, and bcc-Voronoi[001] is the largest, bcc-Voronoi[011] is the second, and bcc-Voronoi[111] is the smallest at same temperature. Yue[27] has roughly explained that the reason for the change in compressive strength under different loading directions is that the compressive strength is affected by the number of struts on compression direction. Summary of cell geometries of AM porous titanium at different loading direction in Table 2. According to the explanation of Yue [28], the reason why bcc-Voronoi[001] is larger than bcc-Voronoi [111] is that the number of oblique struts of bcc-Voronoi[001] is more than bcc-Voronoi[111] because oblique strut have high resistance to the compressive deformation compared to perpendicular strut. But this reason cannot explain why bcc-Voronoi[001] is greater than bcc-Voronoi[011], because the number of oblique struts of bcc-Voronoi[001] equal than the bcc-Voronoi[011]. In order to explain the anisotropy of AM porous titanium in detail, this study uses a finite element analysis method to determine the deformation mechanism under different compression directions. It can be obtained that the deform domination of oblique struts of bcc-Voronoi[001] is yielding dominated, oblique struts of

bcc-Voronoi[011] is yielding dominated and parallel struts is buckling dominated, oblique struts bcc-Voronoi[111] is bending dominated form Hamaguchi [29]. Compared with Hamaguchi, although the model is the same, but the material is aluminum alloy and the manufacturing method is SLM. Compared with aluminum alloy, CP-titanium has a higher Young's modulus, ductility and hardness. B. Dutta [11] also explained that EBM have lower strength and higher ductility than SLM duo to slower cooling. Yielding dominated cell structures show relatively superior strength and stiffness, and thus can be employed to bear the load and strength of bending dominated is relatively low. And compared with bcc-Voronoi[001], the buckling strength of bcc-Voronoi[011] is greater, which is why the plateau stress of bcc-Voronoi[001] is greater than bcc-Voronoi[011]. On the other hand, it can be found from Figure. 4.1 that changes in temperature and porosity will not affect the anisotropy of AM porous titanium, mainly because the mechanism has not changed.

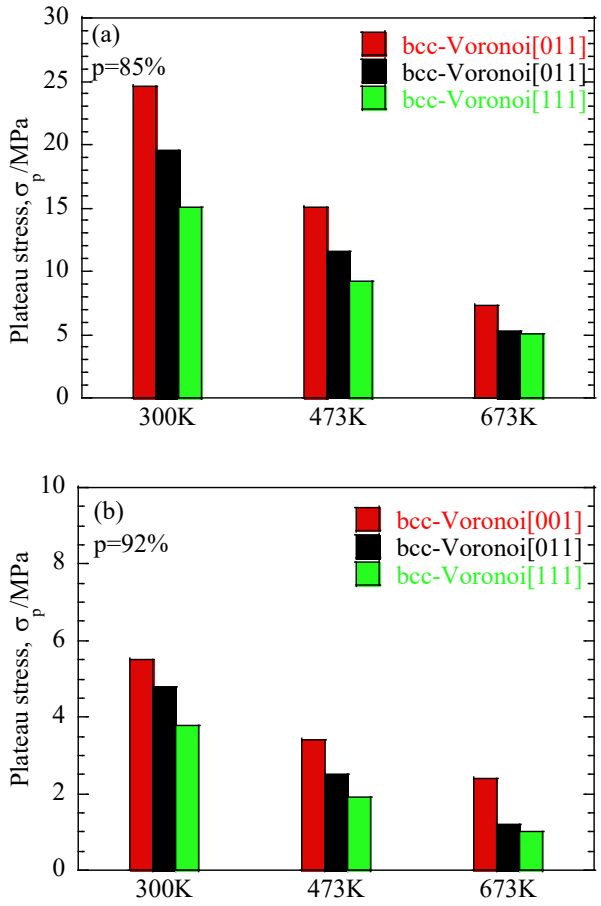


Fig. 4.1 The plateau stress of AM porous titanium with the loading direction and different compressive temperature. (a) porosity of 85%; (b) porosity of 92%.

Table 2 Summary of cell geometries of AM porous titanium at different loading direction.

| **Loading direction** | **Number of** | | |
|---|---|---|---|
| | Parallel struts | Perpendicular struts | Oblique struts |
| **bcc-Voronoi[001]** | 0 | 12 | 24 |
| **bcc-Voronoi[011]** | 6 | 6 | 24 |
| **bcc-Voronoi[111]** | 0 | 18 | 18 |

**4.2 The shear band**

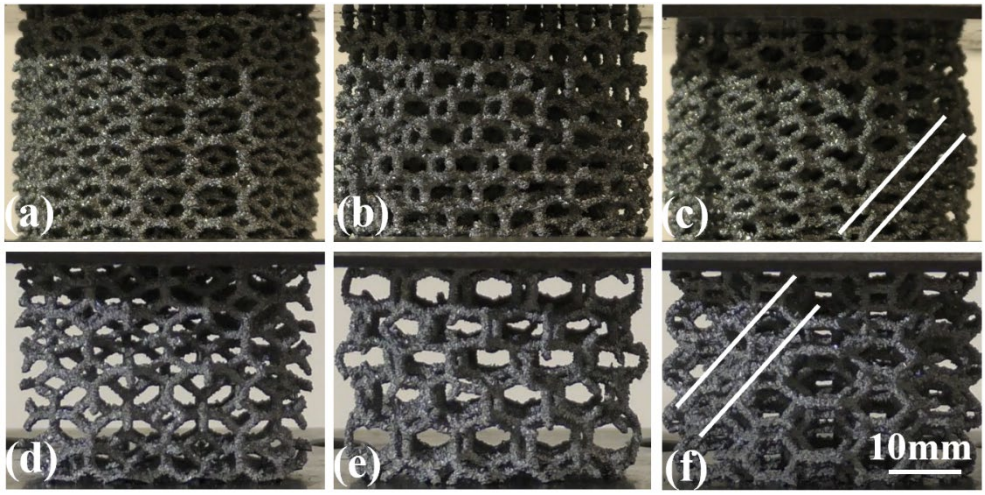


Fig. 4.3 Photographs of compressive specimens with strain of 25% at 300K. Porosities are (a)-(c) 85% and (d)-(f) 92%. Cell structures are bcc-Voronoi (a) (d) [001], (b) (e) [011], (c) (f) [111].

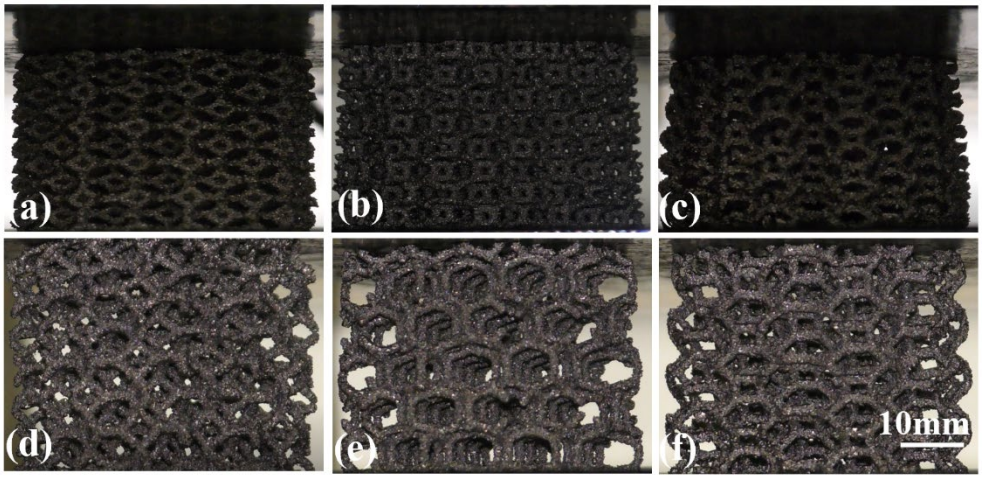


Fig. 4.4 Photographs of compressive specimens with strain of 25% at 473K. Porosities are (a)-(c) 85% and (d)-(f) 92%. Cell structures are bcc-Voronoi (a) (d) [001], (b) (e) [011], (c) (f) [111].

Fig. 4.3 shows the compressive specimens with the strain of 25% of strain and the shear band can be observed at bcc-Voronoi[111]. According to previous research, it can be found that the occurrence of shear band is related to various factors, such as the properties of material, cell structure, and the manufacturing method of the porous material[30, 31]. Base on above experimental result, shear band did not occur in the compression direction of bcc-Voronoi[001] and bcc-Voronoi[011] but shear bands occurred in the compression direction of bcc-Voronoi[111]. Because the deform domination of oblique struts of bcc-Voronoi[001] is yielding dominated, oblique struts of bcc-Voronoi[011] is yielding dominated and parallel struts is buckling dominated, oblique struts bcc-Voronoi[111] is bending dominated.

In contrast, the results of previous studies show that shear band also occur in Ti-6Al-4V at bcc-Voronoi[001], because the ductility of commercial pure titanium is greater than Ti-6Al-4V, and the hardness of commercial pure titanium is lower than Ti-6Al-4V [9]. Research on manufacturing methods, such as the occurrence of shear bands in selective laser melting, is easier than in electron beam melting, because the electron beam melting has lower residual stress [6, 20]. This study also found that the temperature also affects the occurrence of shear band, such as bcc-Voronoi[111] has not occurred at 473K (Fig. 4.4), mainly due to high temperature softening reduces the hardness of material. The existence of shear band reduces the performance of porous material, so avoiding the occurrence of shear bands is also a consideration in the design of porous materials in the future.

### 4.3 Strain rate sensitivity

The relationship between the stress and the initial strain rate can be expressed as [32],

$$\sigma = K\dot{\varepsilon}^m \tag{4}$$

where σ is the plateau stress; K is the constant depending on the temperature; $\dot{\varepsilon}$ is the initial strain rate and m is the value of strain rate sensitivity.

The plateau stress of AM porous titanium with three different temperature in static compression is plotted against strain rate on a logarithmic coordinate in Fig. 4.5 to evaluate the strain rate sensitivity of AM porous titanium. The calculation of strain rate sensitivity as the slop of fitting lines for each temperature and the quantitative experimental results of AM porous titanium. AM porous titanium with porosity of 85% have m-values of 0.020, 0.032 and 0.051 at 300, 473and 673 K, respectively. And AM porous titanium with porosity of 92% are 0.014, 0.028 and 0.045 at 300, 473 and 673 K, respectively. We found that the m-values of porous titanium are very low. The low strain rate sensitivity is due to the property of titanium. According to previous studies, the strain rate sensitivity of closed-cell aluminum foam is usually affected by the rate sensitivity of the base material, shock wave propagation, the compressed air pressure with cells and the micro-inertial [33-35]. The shock wave propagation and the micro-inertial have insignificant contribution to strain rate sensitivity at low strain rates.

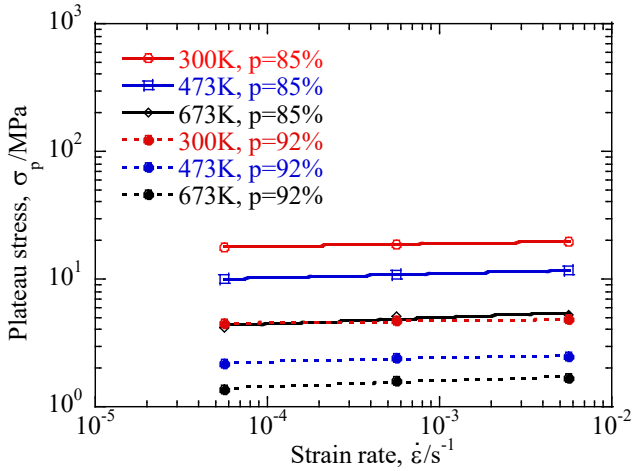


Fig. 4.5 Plateau stress at different temperature of 300K, 473K, 673K is plotted as a function of strain rate with different porosities of AM porous titanium.

### 4.4 Apparent activation energy

High temperature constitutive equation as [36]:

$$\dot{\varepsilon} = A\sigma^n exp\left(-\frac{Q}{RT}\right) \tag{5}$$

where $\dot{\varepsilon}$ is the initial strain rate, σ is the plateau stress, n is the stress exponent, T is the deformation temperature, Q is the apparent activation energy, R is the gas constant, A is the material-dependent constant.

The logarithm of flow stress at a constant strain rate is plotted as a function of 1/T and by regression analysis of Fig. 4.6, the apparent activation energy of AM porous titanium is the slope of the curves can be calculated. Compared with CP-titanium[37] (746 kJ/mol), PM titanium foam [28] (porosity of 60%, 603 kJ/mol) and AM porous titanium (porosity of 85%, 92%, 515 kJ/mol and 502kJ/mol) can obtain the apparent activation energy decreases with an increase of porosity. Fig. 4.7 shows the apparent activation energy plotted against the porosity of porous titanium. Form Fig. 4.7, the apparent activation energy decreases with increase of porosity. Because the microscopic deformation mechanism of AM porous titanium(bcc-Voronoi[011]) were yielding and buckling dominated, while the PM porous titanium were bending and yielding dominated and dense titanium were yielding dominated. Therefore, the structural design of porous metal under high temperature conditions minimizes bending and buckling deformation.

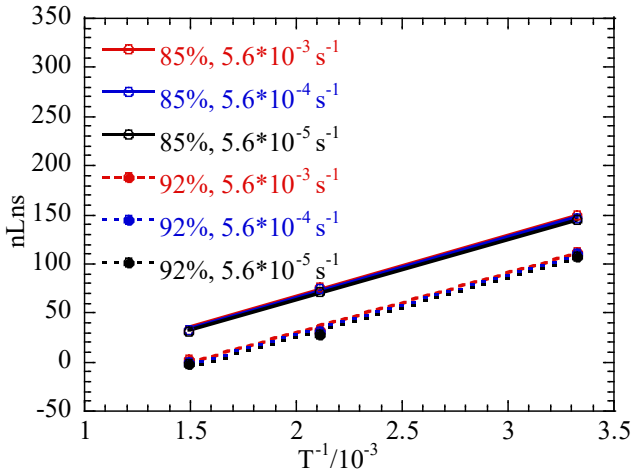


Fig. 4.6 The logarithm of flow stress at 10mm/min is plotted as a function of 1/T with different compression direction and porosity.

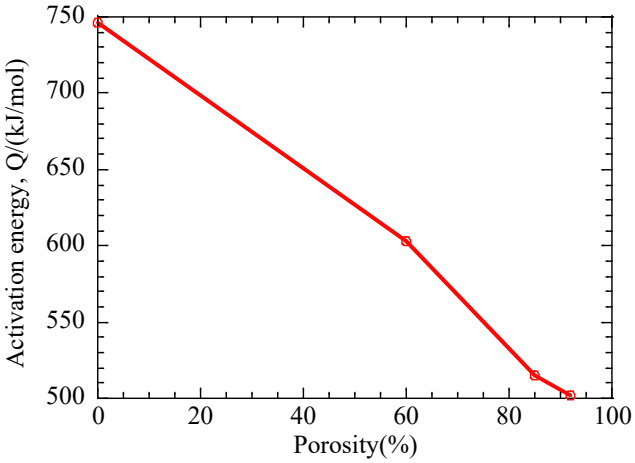


Fig. 4.7 The apparent activation energy plotted against the porosity of porous titanium

## 5. Conclusion and future works

Compression tests of AM porous titanium specimens with bcc-Voronoi cell structure were carried out with different strain rates, temperatures and compression directions. Some specific conclusions have been summarized as:

Plateau stress of ordered open-cell structure was changed as loading direction and this change is not affected by temperature and porosity. The generation of shear band of ordered open-cell porous metal is affected not only by cell structure, properties of material and manufacturing methods but also by temperature. The strain rate sensitivity of ordered open-cell structure was quite low at a low initial strain rate due to the property of matrix material. The temperature dependence of the disordered structure is higher than that of the ordered structure because the low activation energy is due to the dominant deformation of bending and buckling.

In addition, the existence of shear bands and anisotropy has a great impact on the performance of the ordered open-cell structure. Therefore, in the subsequent research of porous materials, it is necessary to consider the avoidance of shear bands and anisotropy, and the temperature of the irregular open-cell structure is higher than the regular open-cell structure. All mentioned above, the irregular structure is our research direction.

**Acknowledgment**

First of all, I would like to extend my sincere gratitude to my supervisor, Professor Koichi Kitazono for his excellent supervision and useful suggestions on my thesis. I deeply thank him for his guidance in completing the two-year master's program at Tokyo Metropolitan University.

It is pleasuring to spend 2 years with my colleagues in Kitazono laboratory who have been capable, helpful and kind during my research study.

Finally, I want to thank my family. I sincerely thank you for your continued support and encouragement.

**REFERENCES**


1) Rodríguez-Galan, I. Sabirow, J. Segurado, Int. J. Plast. 70 (2015) 191-205

2) J.H. Shen, G.X. Lu, D. Ruan. Compressive behaviour of closed-cell aluminium foams at high strain rates. Composites: Part B. 41 (2010) 678-685.

3) Schwingel D, Seeliger H-W, Vecchionacci C, Alwes D, Dittrich J. Aluminium foam sandwich structures for space applications. Acta Astronautica 2007; 61:326-30.

4) Louis-Philippe Lefebvre JB, David C. Dunand. Porous Metals and Metallic Foams: Current Status and Recent Developments. Advanced Engineering Materials 2008; 10:775-87.

5) Ettrich J. Fluid Flow and Heat Transfer in Cellular Solids. Dissertation, Karlsruher Institut für Technologie (KIT): KIT Scientific Publishing; 2014.

6) X.Y. Cheng, S.J. Li, L.E. Murr, Z.B. Zhang, Y.L. Hao, R. Yang, F. Medina, R.B. Wicker. J. Mech. Behav. Biomed. 16 (2012) 153-162.

7) Fabrizio Matassi AB, Luigi Sirleo, Christian Carulli, Massimo Innocenti. Porous metal for orthopedics implants. Clinical Cases in Mineral and Bone Metabolism 2013; 10:111-5.

8) Akiyama S, Ueno H, Imagawa K, Kitahara A, Nagata S, Morimoto K, et al. Foamed metal and method of producing same. Google Patents; 1987.

9) Yue XZ, BY Hur. Fluidity and Mechanical Properties of Open Cell AZ31 Mg Alloy Foam, Journal of Korea Foundry Society. 2012; 3: 150-156.

10) I. G. Papantoniou, D. I. Pantelis, D. E. Manolakos: Procedia Structural Integrity. 10 (2018) 243-248.

11) N.N GUO, M.C. LEU. Additive manufacturing: technology, applications and research needs, Front. Mech. Eng. 8 (2013) 215–243.

12) B.Dutta, F.H. (Sam)Froes. The Additive Manufacturing (AM) of titanium alloys, Metal Powder Report.72 (2017) 96-106.

13) D. Herzog, V. Seyda, E. Wycisk, C. Emmelman: Acta mater. 117 (2016) 371-192.

14) Leitner A, Maier-Kiener V, Jeong J, Abad MD, Hosemann P, Oh SH, et al. Interface dominated mechanical properties of ultra-fine grained and nanoporous Au at elevated temperatures. Acta Materialia 2016; 121:104-16.

15) XZ Yue, K Kitazono, X-J Yue, B-Y Hur. Effect of fluidity on the manufacturing of open cell magnesium alloy foams. Journal of Magnesium and Alloys 2016; 4:1-7.

16) Park JS, Hyun SK, Suzuki S, Nakajima H. Effect of transference velocity and hydrogen pressure on porosity and pore morphology of lotus-type porous copper fabricated by a continuous casting technique. Acta Materialia 2007; 55:5646-54.

17) Melisa Cardona JAI, Juan Fernando Ramírez, Patricia Fernández-Morales. Pores distribution statistical analysis for metal foams obtained by casting-dissolution process. Revista Matéria 2016;21: pp.501-9.

18) Szyniszewski S, Smith BH, Hajjar JF, Arwade SR, Schafer BW. Local buckling strength of steel foam sandwich panels. Thin-Walled Structures 2012; 59:11-9.

19) Liu YJ, Wang HL, Li SJ, Wang SG, Wang WJ, Hou WT, et al. Compressive and fatigue behavior of beta-type titanium porous structures fabricated by electron beam melting. Acta Materialia 2017; 126:58-66.

20) D. Rodríguez-Galan, I. Sabirow, J. Segurado, Int. J. Plast. 70 (2015) 191-205.

21) Haynes WM. CRC handbook of chemistry and physics, 95th Edition. CRC PRESS 1947.

22) Krebs RE. The history and use of our earth`s chemical elements: a reference guide: Greenwood Publishing Group; 2006.

23) Ahmadi S, Yavari S, Wauthle R, Pouran B, Schrooten J, Weinans H, et al. Additively Manufactured Open-Cell Porous Biomaterials Made from Six Different Space-Filling Unit Cells: The Mechanical and Morphological Properties. Materials 2015; 8:1871.

24) S. Zhao, S.J. Li, W.T. Hou, Y.L. Hao, R. Yang, R.D.K. Misra. J. Mech. Behave. Biomed. 59 (2016) 251-164.

25) S.M Ahmadi, G. Campoli, S. Amin Yavari, B. Sajadi, R. Wauthle, J.Schrooten, H. Weinans, A.A. Zadpoor. J. Mech. Behave. Biomed. 34(2014) 106-115.

26) L.J. Xiao, W.D. Song, C. Wang, H.Y. Liu. H.P. Tang, J.Z. Wang. Mater. Sci. Eng. A 640 (2015) 375-384.

27) X. Yue, K. Matsuo, K. Kitazono. Mater. Trans. 58 (2017), 1587-1592.

28) X. Yue, H. Fukazawa, K. Kitazono. Mater. Sci. Eng. A, 673 (2016), 83-89.

29) T. Hamaguchi, Y. Fujimori, C. Matsuo, K. Kitazono: The proceedings of the 2018 Japanese spring conference for the technology of plasticity, 2018.

30) O.E. Sotomayor, H.V. Tippur. Int J Solids Struct. 51 (2014) 3776-3786

31) L.J. Xiao, W.D. Song, C. Wang, H.Y. Liu. H.P. Tang, J.Z. Wang. Mater. Sci. Eng. A 640 (2015) 375-384.

32) L.J. Xiao, W.D. Song. Int J Impact Eng. 111(2018) 255-272.

33) ISO 20032: 2013, Method for Evaluation of Tensile properties of Metallic Superplastic Materials.

34) Liu YD, Yu JL, Zheng ZJ, Li JR (2009) A numerical study on the rate sensitivity of cellular metals. Int J Solids Struct 46:3988–3998

35) Elnasri I, Pattofatto S, Zhao H, Tsitsiris H, Hild F, Girard Y (2007) Shock enhancement of cellular structures under impact loading: part I Experiments. J Mech Phys Solids 55:2652–2671

36) Pattofatto S, Elnasri I, Zhao H, Tsitsiris H, Hild F, Girard Y (2007) Shock enhancement of cellular structures under impact loading: part II analysis. J Mech Phys Solids 55:2672–2686.

37) M. F. Ashby, A. Evans, N. A. Fleck, L. J. Gibson, J. W. Hutchinson, H. N. G. Wadley: Metal Foams: A Design Guide, (Butterworth-Heinemann, Boston, 2000) pp. 33-34.

38) M.F. Ashby, Acta Metall. 20 (1972) 887-897.

**Appendix A. Conference**

1. Shiyue Guo, Xuezheng Yue, Koichi Kitazono, Effect of ordered cellular structures on high temperature deformation behavior of additively manufactured porous titanium, The 137th Autumn Meeting of the Japan Institute of Light Metals.

**Appendix B. Publication**

1. Shiyue Guo, Xuezheng Yue, Koichi Kitazono, High temperature deformation of additively manufactured porous titanium with ordered cell structures, Material Transaction, in progress.